Aggregation of an Amphiphilic Poly(*p*-phenylene) in Micellar Surfactant Solutions. Small-Angle Neutron Scattering

Tobias Fütterer, Thomas Hellweg,* and Gerhard H. Findenegg

Stranski-Laboratorium für Physikalische und Theoretische Chemie, Technische Universität Berlin, Strasse des 17.Juni 112, D-10623 Berlin, Germany

Jörg Frahn and A. Dieter Schlüter

Institut für Chemie/Organische Chemie, Freie Universität Berlin, Takustr. 3, D-14195 Berlin, Germany

Received February 15, 2005; Revised Manuscript Received June 20, 2005

ABSTRACT: Mixed aggregates of a short-chain nonionic amphiphilic poly(*p*-phenylene), in which each benzene ring of the aromatic backbone is 2,5-disubstituted with a hydrophobic and a hydrophilic group, and of the nonionic surfactant C_8E_4, $C_{12}E_6$, or $C_{10}G_2$ were studied in aqueous solutions. Cryo-transmission electron microscopy and light scattering experiments revealed the existence of fiberlike aggregates of mean length greater 200 nm and a diameter of ca. 6 nm in an excess of small surfactant micelles in these solutions. In the present contribution small-angle neutron scattering (SANS) is used to characterize the fiber aggregates in these complex liquids with respect to their composition and their radial scattering length density distribution $\sigma(r)$. The composition of the fiber aggregates (polymer-to-surfactant number ratio) was determined using perdeuterated surfactant and contrast variation of the solvent (H_2O/D_2O). Moreover, the diameter of the mixed aggregates is determined using form factors for descriptions of the scattering curves and additionally numerical approaches to treat the data. The ratio of surfactant molecules to PPP was found to be 3:1 (20 wt %:80 wt %).

I. Introduction

The peculiar electronic structure of poly(*p*-phenylene)s (abbreviated as PPP) makes these polymers promising candidates for applications in photo- and electroluminescent devices.[1−6] PPPs have an intrinsically stiff linear backbone. Aqueous solutions of amphiphilically substituted nonionic PPP oligomers, in which each benzene ring of the aromatic backbone is substituted with an alkyl chain ($-C_{12}H_{25}$) and an oxyethylene chain ($-CH_2(OC_2H_4)_3OMe$) in the para position to the alkyl substituent are interesting since the structure of the PPPs suggests a rich self-assembly behavior. To our knowledge, only a few systems were studied until now (e.g., refs 7−10). The PPP investigated here was found to be insoluble in water but soluble in solutions of nonionic surfactants forming long cylindrical aggregates (similar to the PPP-sulfonate polyelectrolytes studied by Bockstaller et al.[11,12]). These structures were already characterized using cryogenic transmission electron microscopy (cryo-TEM) and different light scattering techniques.[13,14] Also in several other cases these methods were successfully applied to investigate complex colloidal systems.[15−18] However, these techniques are not able to allow for the determination of the surfactant content in these mixed aggregates. Small-angle neutron scattering (SANS) experiments using the method of contrast variation is an excellent tool for this purpose. Moreover, in the present contribution SANS will also be used to obtain information about the cross-sectional radius, R_{CS}, of the aggregates. This quantity is difficult to extract from light scattering data, and cryo-TEM does not provide an ensemble average and no precise data in the entire length scale. The form-factor-based analysis of the extracted SANS intensity $I(q)_{fiber}$ of the fiber aggregates and the indirect Fourier transformation method (IFT) applied to the extracted $I(q)_{fiber}$ yield R_{CS} and the radial scattering length density distribution $\sigma(r)$ of the fiber aggregates.

II. Samples and Experimental Setup

A. Materials. The polymer PPP(12) studied in this work was synthesized by the transition-metal-catalyzed Suzuki step-growth polymerization technique described elsewhere.[19−21] The sample was characterized by gel permeation chromatography (GPC) which yielded a number- and mass-average molar mass of $M_n = 5200$ g/mol ($n_n = 12$) and $M_w = 8700$ g/mol ($n_w = 21$), corresponding to a ratio $M_w/M_n = 1.7$.

The surfactant tetra(oxyethylene)monooctyl ether (C_8E_4) was purchased from Nikko Chemicals Co., Japan (>99% purity). A perdeuterated sample of this surfactant (d-C_8E_4) was provided by R. K. Thomas, Oxford, UK (>98% purity, ratio D/(D + H) > 0.98). The surfactant hexa(oxyethylene)monododecyl ether ($C_{12}E_6$) was purchased from Nikko Chemicals Co., Japan (>99% purity).

High-purity water from a Milli-Q water purification system (Millipore/Waters) and D_2O from Eurisotop (Saclay, France, ratio D/(D + H) > 0.998) was used as the solvent for the small-angle neutron scattering experiments.

B. Sample Preparation. Solutions of the polymer PPP-(12) in aqueous media were prepared by adding 0.05−0.4 wt % of the polymer to 0.5−4 wt % micellar solutions of the surfactants C_8E_4 or $C_{12}E_6$ in water. The pure surfactant solutions were filtered (pore size 200 nm; Schleicher & Schuell) directly into the sample cells (quartz, Hellma, Germany); after addition of the polymer the mixtures are treated in an ultrasonic bath (35 kHz) for at least 2 h at ca. 45 °C. At this elevated temperature the aqueous systems are phase separated into a surfactant-rich and a dilute aqueous phase. After remixing and equilibration at room temperature the clear

* To whom correspondence should be addressed. E-mail: thomas.hellweg@tu-berlin.de.

10.1021/ma050323l CCC: $30.25
Published on Web 07/26/2005

solutions were investigated without further filtering to avoid concentration changes of the samples.

C. Small-Angle Neutron Scattering. The SANS measurements with C_8E_4 and $C_{12}E_6$ as the surfactants in pure D_2O were performed at the beamline V4 of the reactor BERII at the Hahn-Meitner-Institut (HMI) Berlin, Germany[22] (mechanical selector; wavelength $\lambda_0 = 0.6$ nm, $\Delta\lambda_0/\lambda_0 = 0.1$; sample−detector distance: 1, 4, and 16 m; ^{3}He detector (64 × 64 elements); Hellma quartz cells (1 mm); standard: H_2O) and at the beamline D11 of the high flux research reactor at the Institut-Laue-Langevin (ILL) in Grenoble, France[23] (mechanical selector; wavelength $\lambda_0 = 1.0$ nm, $\Delta\lambda_0/\lambda_0 = 0.1$; sample−detector distance: 2, 8, and 36 m; ^{3}He detector (64 × 64 elements); Helma quartz cells (1 mm); standard: H_2O). The SANS matching experiments with d-C_8E_4 as the surfactant in D_2O/H_2O mixtures were carried out at the beamline KWS1 at the Forschungszentrum Jülich (FZJ), Germany (mechanical selector; wavelength $\lambda_0 = 0.6$ nm, $\Delta\lambda_0/\lambda_0 = 0.1$; sample−detector distance: 1.25, 2, and 8 m; ^{3}He detector (64 × 64 elements); Helma quartz cells (1 mm); standard: calibration according to ref 24).

The measured SANS intensities were corrected for the efficiency of the different detector cells and were circularly averaged. After correction for the scattering of the solvent and the empty cell, the data were brought to absolute scale. All data reduction steps were performed using the standard software provided by the individual institutes.

III. SANS Data Analysis and Results

In general, small-angle scattering curves from colloidal solutions can be represented by

$$I(q) = C\Delta\sigma^2 P(q)S(q) \tag{1}$$

where C is a concentration-dependent factor and $\Delta\sigma$ is the excess scattering length density of the particles ($\Delta\sigma = \sigma_{\text{particle}} - \sigma_{\text{solvent}}$). For low concentrations and intermediate or large values of q $S(q) \approx 1$; hence, the analysis of the SANS experiments has mainly to deal with the particle form factor.[25,26]

A. Polymer-to-Surfactant Ratio. Besides the characterization of the size and shape of the fiberlike particles, it is of interest to determine the composition of the aggregates in the present self-assembled multicomponent system. A method to determine the intensity of one component in a mixed system with high accuracy is based on contrast variation in SANS experiments.

In the case of two different types of scattering particles this application of contrast-variation SANS requires a sufficiently large difference in the scattering length density of the two different species contributing to the total scattering intensity. In neutron scattering experiments this is usually achieved by employing deuterated compounds. A fully deuterated surfactant, d-C_8E_4, was used to generate the contrast difference between the micelles and fiber aggregates.

The scattering intensity at a given q value (say q') is a function of the concentration and the contrast between solvent to particle. For two different types of particles, $I(q')$ is the sum of the two contributions. q' has to be chosen such that one can monitor the particle as a homogeneous body with some mean scattering length density, defined by the real scattering length density distribution. For the present system at a value of $q' = 0.1$ nm^{-1}, the cluster contribution can be neglected, and the form factors $P(q')$ of the micelles and fiber aggregates are causing no intraparticle interference effects on $I(q')$. For given concentrations the total scattering intensity $I(q' = 0.1\ \text{nm}^{-1})$ of the fibers and the micelles is a function of the contrast $\Delta\sigma$ (or of the scattering length density of the solvent $\sigma_{\text{solvent}}(x_{D_2O})$) and can be written as

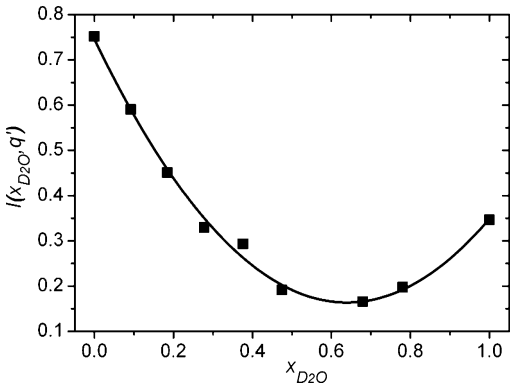

Figure 1. Total SANS intensity at $q' = 0.1$ nm^{-1} as a function of the mole fraction x_{D_2O} for a solution of 0.2 wt % PPP(12) and 2 wt % d-C_8E_4 in mixtures of H_2O and D_2O (symbols) and a fit according to eq 2 (line). The errors of $I(q')$ are indicated by the size of the symbols.

$$I(x_{D_2O},q') = C_{\text{fiber}}{}^*(\sigma_{\text{fiber}} - \sigma_{\text{solvent}})^2 + C_{\text{micelle}}{}^*\Delta\sigma_{\text{micelle}}{}^2 \tag{2}$$

where x_{D_2O} is the mole fraction of D_2O in the H_2O/D_2O solvent mixture and C^*_{particle} is a concentration-dependent factor. The scattering length density of the H_2O/D_2O solvent mixture can be calculated from the known mole fraction x_{D_2O} and the scattering length densities of pure H_2O and D_2O. The scattering length density of the pure d-C_8E_4 micelles can also be calculated ($\sigma_{d-C_8E_4} = 7.1 \times 10^{-6}$ Å^{-2}).[27] By fitting eq 2 to the scattering data for a wide range of x_{D_2O} of the H_2O/D_2O solvent mixture, the parameters C^*_{fiber}, σ_{fiber}, and C^*_{micelle} can be determined. The parameter C^*_{micelle} can be determined independently from the scattering intensity of d-C_8E_4 solutions in the absence of the polymer. With the assumption that $P(q')_{\text{micelle}}$ has the same value in the absence and presence of the polymer and that $S(q')_{\text{mix}} \approx S(q')_{\text{pure}}$, the ratio of $C^*_{\text{micelle,mix}}$ to $C^*_{\text{micelle,pure}}$ yields the amount of dissolved surfactant which is incorporated in the fiber aggregates.

In Figure 1 the measured total scattering intensity $I(q)$ at $q = 0.1$ nm^{-1} of 0.2 wt % PPP(12) and 2 wt % d-C_8E_4 in mixtures of H_2O and D_2O is plotted in dependence on the mole fraction of D_2O in the solvent. $I(q = 0.1\ \text{nm}^{-1})$ is determined by a linear fit of $I(q)$ in the q range $0.08 < q < 0.2$ nm^{-1} and then calculating $I(q = 0.1\ \text{nm}^{-1})$ from these fit results. A fit of eq 2 to the data is shown in Figure 1. It can be seen that the measured dependence of I on the contrast is described with good accuracy by this relation. The fitting leads to the concentration dependent factor C^*_{micelle} and with complementary data for d-C_8E_4 solutions without polymer, we derive a surfactant-to-polymer number ratio of 3:1, corresponding to a surfactant-to-polymer mass ratio of 1:4. However, the error limits of this determination are high, about 100%, due to the fact that only a small fraction of the dissolved surfactant is incorporated into the fiber aggregates. Accordingly, $C^*_{\text{micelle,mix}}$ and $C^*_{\text{micelle,pure}}$ differ by no more than 4%, and the error in the determination of C^*_{micelle} is 2% (from the fit for $C^*_{\text{micelle,mix}}$ and from the measurement for $C^*_{\text{micelle,pure}}$).

B. Cross Section of the Fiber Aggregates. To gain further structural information about the fiber aggregates, SANS measurements on solutions of PPP(12) in nondeuterated C_8E_4/D_2O and nondeuterated $C_{12}E_6/D_2O$

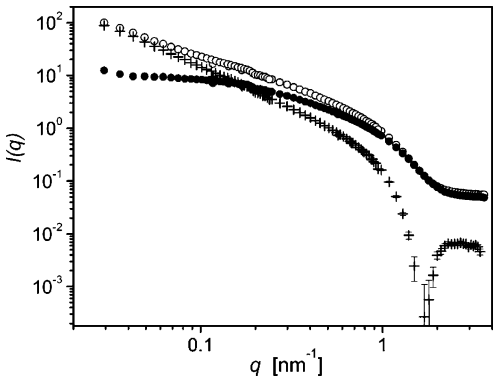

Figure 2. Absolute scattering curves $I(q)$ of (a) a 0.3 wt % PPP(12) plus 2 wt % C_8E_4 solution (open cycles) and (b) a 2 wt % C_8E_4 solution (full cycles), both in D_2O. The crosses indicate the difference of (a) and (b) with an appropriate correction factor (see text).

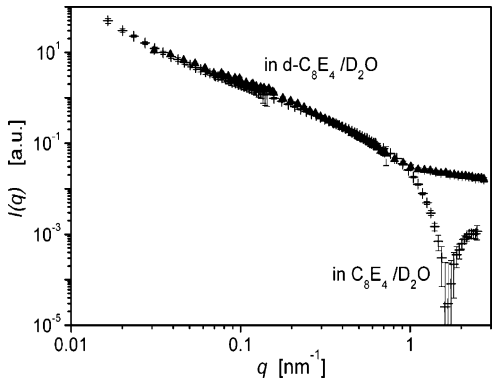

Figure 3. Comparison of the difference curve representing the fiber contribution (crosses, see Figure 2) with the directly measured scattering curve with fully deuterated d-C_8E_4 as the surfactant (black symbols). Micelles of deuterated d-C_8E_4 are nearly completely matched by the solvent (D_2O), and thus scattering is almost solely due to the fiber aggregates.

were performed and compared with the scattering curve $I(q)_{\text{micelle,pure}}$ of a sample of the same surfactant concentration in the absence of the polymer. The total scattering intensity of the PPP/surfactant solution can be represented by a sum of the individual scattering contributions (again with $S(q) \approx 1$). The measured "blank curve" $I(q)_{\text{micelle,pure}}$ was subtracted from the scattering curve of the polymer plus surfactant solutions, taking into account that in the latter a small fraction of surfactant does not exist in form of free micelles but is incorporated into the fiber aggregates. In the present case, this fraction is ca. 4% for the PPP(12)/C_8E_4 sample and ca. 13% for the PPP(12)/$C_{12}E_6$ sample as determined by the SANS contrast variation experiments. Accordingly, on subtracting the scattering contribution caused by the surfactant micelles, the scattering curve of the pure surfactant solution is taken with a correction factor $x = 0.96$ and 0.87, respectively. The scattering intensity from the fiber aggregates is given by

$$I(q)_{\text{fiber}} = I(q)_{\text{total}} - xI(q)_{\text{micelle,pure}} \tag{3}$$

Figure 2 shows an example of the subtraction process. To test the justification of this procedure, we compare a difference curve with the scattering curve of a mixture with perdeuterated d-C_8E_4/PPP(12) in pure D_2O. This comparison is shown in Figure 3. The scattering length density of the pure d-C_8E_4 micelles nearly equals the scattering length density of D_2O, and thus the contribution of the micelles can be neglected in this case. In the low-q region the two curves in Figure 3 agree within the limits of error. The difference curve in Figure 2 and subsequent figures exhibit a pronounced minimum near $q = 1.5$ nm^{-1} as to be expected for the form factor of cylinders. However, for a real experiment such a sharp minimum is not expected even for cylindrical particles of perfectly monodisperse cross section due to imperfect beam collimation and the wavelength distribution of the neutron beam. The sharpness of the minimum is likely to be an artifact in the subtraction of the two scattering curves. Assuming a slightly lower correction factor for the scattering curve of the pure surfactant solution (corresponding to a somewhat higher surfactant-to-polymer ratio in the fiber aggregates) would lead to a smeared (less sharp) minimum in the difference curve. However, these details have no significant effect on the analysis of the difference curves with respect the cross-sectional radius R_{CS} and the radial scattering length density distribution $\sigma(r)$.[27]

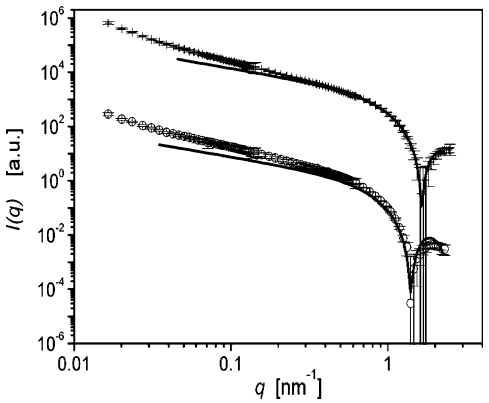

Figure 4. Difference curve representing the fiber contribution for a solution of 0.2 wt % PPP(12) and 2 wt % C_8E_4 (crosses) and a solution of 0.3 wt % PPP(12) and 2 wt % $C_{12}E_6$ (open symbols) in D_2O. The lower curve is shifted by a factor of 10^{-5}. The solid lines are fits by a form factor of a homogeneous cylinder.

Table 1. Cross-Sectional Radius R_{CS} of the Fiber Aggregates from the Fits with the Form Factor of a Homogeneous Cylinder, $R_{\text{CS,hom}}$, from the Pair Distance Distribution Function $p(r)$ (Eq 4), $R_{\text{CS,equi}}$, and from the Cryo-TEM Micrographs, $R_{\text{CS,TEM}}$

PPP(12) in	$R_{\text{CS,hom}}$ [nm]	$R_{\text{CS,equi}}$ [nm]	$R_{\text{CS,TEM}}$ [nm]
C_8E_4	2.35 ± 0.1	2.3 ± 0.1	2.9 ± 0.2
$C_{12}E_6$	2.75 ± 0.1	2.6 ± 0.1	3.2 ± 0.3

To determine the cross-sectional radius and the radial scattering length density distribution of the fiber aggregates, we analyzed the extracted SANS intensity of the fiber aggregates $I(q)_{\text{fiber}}$. Figure 4 shows a fit of the difference curve for fiber aggregates of PPP(12) in micellar solution of C_8E_4 and of $C_{12}E_6$, both in D_2O, by the model form factor of a homogeneous cylinder. The cross-sectional radius of the fiber aggregates, $R_{\text{CS,hom}}$, derived from this fit is $R_{\text{CS,hom}} = 2.35$ nm for the PPP(12)/C_8E_4 solution and $R_{\text{CS,hom}} = 2.75$ nm for the PPP(12)/$C_{12}E_6$ solution (see Table 1). The increased value for the system with the longer surfactant indicates a radial incorporation of the surfactant molecules into the fiber aggregates. The model-independent analysis of the fiber cross section according to the indirect Fourier transformation method by Glatter[28−30] yields the radial pair distance distribution function $p(r)$, and the Fourier transform of $p(r)$ represents $I(q)_{\text{fit}}$ for the high-q range. For the system with the surfactant C_8E_4 the resulting

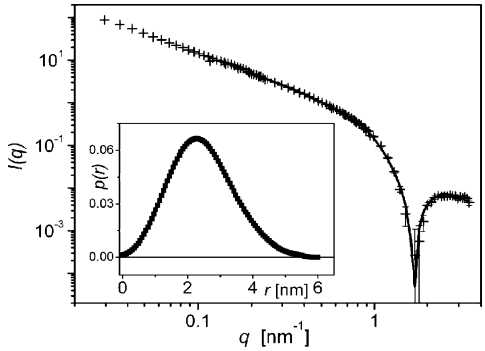

Figure 5. Difference curve representing the fiber contribution for a 0.2 wt % PPP(12) plus 2 wt % C_8E_4 solution in D_2O (crosses). The line represents the Fourier transform of the pair distance distribution function $p(r)$. Inset: pair distance distribution function $p(r)$ obtained by indirect Fourier transformation of the measured data.

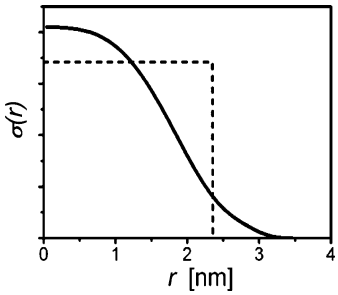

Figure 6. Radial excess scattering length density distribution function obtained by deconvolution of $p(r)$ of the fiber aggregates for a solution of 0.2 wt % PPP(12) and 2 wt % C_8E_4 in D_2O. The dashed line indicates $R_{CS,hom}$ according to a box model of a homogeneous cylinder.

radial $p(r)$ curve and the respective $I(q)_{fit}$ are shown in Figure 5. The shape of $p(r)$ indicates a radial-symmetric cross section for the fiber aggregates. From $p(r)$ an equivalent homogeneous radius $R_{CS,equi}$ can be calculated according to[31]

$$R_{CS,equi}{}^2 = \frac{\int_0^\infty p(r) r^2 \, dr}{\int_0^\infty p(r) \, dr} \tag{4}$$

For both polymer/surfactant systems the calculated radii $R_{CS,equi}$ agree with $R_{CS,hom}$ from the form factor analysis (see Table 1).

The radial scattering length density distribution function is the deconvolution of $p(r)$. In Figure 6 the resulting radial scattering length density is shown for PPP(12)/C_8E_4/D_2O as an example. For both systems the excess scattering length density has a maximum for the core of the fiber aggregates and decreases monotonically in the shell region of the fiber aggregates, i.e., a core−shell arrangement with the alkyl chains pointing inward the aggregates and the oxyethylene groups pointing to the aqueous medium. The maximum dimension of R_{CS} for PPP(12)/C_8E_4/D_2O and for PPP(12)/$C_{12}E_6$/D_2O are in good agreement with the observed values of R_{CS} from the cryo-TEM investigations and with the calculated length of a PPP(12) monomer in the all-trans configuration of 3.2 nm (see Table 1 and ref 13).

IV. Model for the Internal Structure of the Fiber Aggregates

The results presented above lead to a structural model for the fiber aggregates. The radial scattering length density profile $\sigma(r)$ is typical for a radial symmetric core−shell arrangement of amphiphiles in aqueous solution, like e.g. wormlike micelles of $C_{12}E_5$ in H_2O.[32] The dependence of R_{CS} on the length of the surfactant points to a radial incorporation of the surfactant molecules into the fiber aggregates. The role of the surfactant could be an increase of the natural curvature of a polymer layer to allow for the formation of cylindrical aggregates, which exhibit an increased curvature compared to the lamellar phase observed for the bulk structure of PPP(12).[13] The determined radial aggregation number is $N_{rad} = 19$,[14] and the number ratio PPP(12)$_{monomer}$ to surfactant is 15:4 for the cross section. It is impressive that this short polymer PPP(12), exhibiting a backbone length of only 5 nm, is able to form stiff self-assembled cylindrical structures with length $L \approx$ 500 nm. This is explained by a lengthwise displacement of the polymer backbones along the fiber axis. Figure 7 shows a schematic illustration of the probable structure.

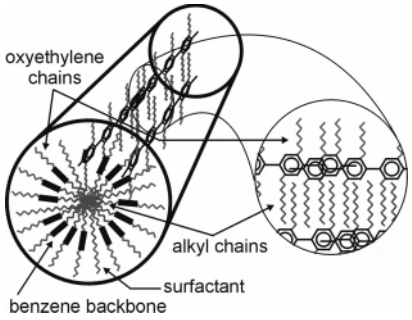

Figure 7. Sketch of the proposed structure of the fiber aggregates illustrating the radial arrangement of the PPP-(12) and surfactant molecules (left) and the lengthwise displacement of the polymer backbones along the fiber axis (right). We included only two PPP chains along the fiber axis due to visual reasons. The determined radial aggregation number of $N_{rad} = 15$ for the PPP molecules is only shown in the cross section (left).

V. Conclusion

The comicellization of a nonionic amphiphilic 2,5-disubstituted poly(*p*-phenylene) with nonionic surfactants in aqueous solutions was studied by means of small-angle neutron scattering techniques. The focus of the present article was to gain insight into the local or short scale structure of the formed colloidal aggregates in the presence of an excess of other particles also exhibiting colloidal size (i.e., excess surfactant micelles).

The cross-sectional radius R_{CS} of the fiber aggregates was determined by SANS. We show that the contribution of the surfactant micelles to the scattering intensity can be subtracted from the overall scattering curve $I(q)$, while the contribution of the cluster aggregates (see part I, ref[1y]) does not contribute to the scattering in the high q range of the SANS experiments. The resulting $I(q)_{fiber}$ difference curve containing the information about the fiber aggregates was analyzed by two different methods, viz., using a model of homogeneous cylinders, and by the indirect Fourier transformation method via the pair distance distribution function. The two values of R_{CS} derived by these different approaches in the SANS data analysis are equal within the error limits, and they are consistent with the diameter of the fiber aggregates derived from cryo-TEM.[21] On the other hand, a somewhat larger value of R_{CS} was found for fiber aggregates with $C_{12}E_6$ as compared with fiber aggregates containing C_8E_4. The radial scattering length density distri-

bution $\sigma(r)$ of the fiber aggregates corresponds to a core−shell structure, such that the hydrophobic and hydrophilic side chains are pointing inward and outward, respectively, reminiscent of a cylindrical surfactant micelle.

The amount of surfactant contained in the fiber aggregates was determined by SANS contrast matching experiments, using fully deuterated surfactant and a set of H_2O/D_2O mixtures of different relative content of D_2O, to attain different contrasts of the surfactant micelles and fiber aggregates against the solvent. For the aggregates of PPP(12) with the surfactant C_8E_4 a number ratio of surfactant to polymer molecules of 3:1 was found, though the limits of experimental error are rather high.

Combination of the present results with the previously obtained data from cryo-TEM and light scattering allowed the suggestion of a structural model for the fiber aggregates.

Acknowledgment. The authors are grateful to A. Brandt (HMI Berlin), C. Dewhurst (ILL Grenoble), and W. Pyckhout-Hintzen (FZ Jülich) for help with the SANS measurements and thank the Hahn-Meitner-Institut, the Institute Laue-Langevin, and the Forschungszentrum Juelich for providing neutron beamtime. Financial support from the Deutsche Forschungsgemeinschaft (DFG) through SFB 448, and complementary support through the Fonds der Chemischen Industrie, is also gratefully acknowledged.

References and Notes

(1) Kranzelbinder, G.; Byrne, H. J.; Hallstein, S.; Roth, S.; Leising, G.; Scherf, U. *Phys. Rev. B* **1997**, *56*, 1632−1636.
(2) Savvateev, V. N.; Yakimov, A.; Davidov, D. *Adv. Mater.* **1999**, *11*, 519−531.
(3) Grice, A. W.; Bradley, D. D. C.; Bernius, M. T.; Inbasekaran, M.; Wu, W. W.; Woo, E. P. *Appl. Phys. Lett.* **1998**, *73*, 629−631.
(4) Harrison, B. S.; Foley, T. J.; Bouguettaya, M.; Boncella, J. M.; Reynolds, J. R.; Schanze, K. S.; Shim, J.; Holloway, P. H.; Padmanaban, G.; Ramakrishnan, S. *Appl. Phys. Lett.* **2001**, *79*, 3770−3772.
(5) Pan, J.; Scherf, U.; Schreiber, A.; Haarer, D. *J. Chem. Phys.* **2000**, *112*, 4305−4309.
(6) Neher, D. *Adv. Mater.* **1995**, *7*, 691−702.
(7) Bo, Z.; Zhang, Ch.; Severin, N.; Rabe, J. P.; Schlüter, A. D. *Macromolecules* **2000**, *33*, 2688−2694.
(8) Engelking, J.; Wittmann, M.; Rehahn, M.; Menzel, H. *Langmuir* **2000**, *16*, 3407−3413.
(9) Bo, Z.; Rabe, J. P.; Schlüter, A. D. *Angew. Chem., Int. Ed.* **1999**, *38*, 2370−2372.
(10) Liu, T.; Rulkens, R.; Wegner, G.; Chu, B. *Macromolecules* **1998**, *31*, 6119−6128.
(11) Bockstaller, M.; Köhler, W.; Wegner, G.; Fytas, G. *Macromolecules* **2001**, *34*, 6353−6358.
(12) Bockstaller, M.; Köhler, W.; Wegner, Vlassopoulos, D.; G.; Fytas, G.; *Macromolecules* **2001**, *34*, 6359−6366.
(13) Fütterer, T.; Hellweg, T.; Findenegg, G. H.; Frahn, J.; Schlüter, A. D.; Böttcher, C. *Langmuir* **2003**, *19*, 6537−6544.
(14) Fütterer, T.; Hellweg, T.; Findenegg, G. H.; Frahn, J.; Schlüter, A. D. *Macromolecules* **2005,** *38*, 7443−7450.
(15) Schönfelder, E.; Hoffmann, H. *Ber. Bunsen-Ges. Phys. Chem.* **1994**, *98*, 842−852.
(16) Würtz, J.; Hoffmann, H. *J. Colloid Interface Sci.* **1995**, *175*, 304−317.
(17) Won, Y.-Y.; Brannan, A. K.; Davis, H. T.; Bates, F. S. *J. Phys. Chem. B* **2002**, *106*, 3354−3364.
(18) Nordskog, A.; Egger, H.; Findenegg, G. H.; Hellweg, T.; Schlaad, H.; Berlepsch, H. v.; Boettcher, C. *Phys. Rev. E* **2003**, *68*, 011406/1−011406/14.
(19) Frahn, J.; Schlüter, A. D. *Synthesis* **1997**, *11*, 1301−1304.
(20) Frahn, J. Ph.D. Thesis, Freie Universität Berlin, Berlin, Germany, 1999.
(21) Schlüter, A. D. *J. Polym. Sci., Part A: Polym. Chem.* **2001**, *39*, 1533−1556.
(22) Keiderling, U.; Wiedenmann, A. *Physica B* **1995**, *213&214*, 895−899.
(23) Lindner, P. *Physica B* **1992**, *180&181*, 967−972.
(24) Pyckhout-Hintzen, W.; Springer, T.; Forster, F.; Gronski, W.; Frischkorn, C. *Macromolecules* **1991**, *24*, 1269−1274.
(25) Gradzielski, M.; Langevin, D.; Farago, B. *Phys. Rev. E* **1996**, *53*, 3900−3919.
(26) Hellweg, T.; Langevin, D. *Physica A* **1999**, *264*, 370−387.
(27) Fütterer, T. Ph.D. Thesis, Technische Universität Berlin, Berlin, Germany, 2004.
(28) Glatter, O. *Acta Phys. Aust.* **1977**, *47*, 83−102.
(29) Glatter, O. *J. Appl. Crystallogr.* **1980**, *13*, 7−11.
(30) Glatter, O.; Strey, R.; Schubert, K.-V.; Kaler, E. W. *Ber. Bunsen-Ges. Phys. Chem.* **1996**, *100*, 323−335.
(31) Glatter, O.; Kratky, O. *Small Angle X-Ray Scattering*; Academic Press: London, 1982.
(32) Menge, U.; Lang, P.; Findenegg, G. H.; Strunz, P. *J. Phys. Chem. B* **2003**, *107*, 1316−1320.

MA050323L